# Impact of uncertainties in atmospheric mixing on simulated UTLS composition and related radiative effects

M. Riese,[1] F. Ploeger,[1] A. Rap,[2] B. Vogel,[1] P. Konopka,[1] M. Dameris,[3] and P. Forster[2]

Received 7 March 2012; revised 31 May 2012; accepted 10 July 2012; published 23 August 2012.

[1] The upper troposphere/lower stratosphere (UTLS) region plays an important role in the climate system. Changes in the structure and chemical composition of this region result in particularly large changes in radiative forcings of the atmosphere. Quantifying the processes that control UTLS composition (e.g., stratosphere-troposphere exchange) therefore represents a crucial task. We assess the influence of uncertainties in the atmospheric mixing strength on global UTLS distributions of greenhouse gases (water vapor, ozone, methane, and nitrous oxide) and associated radiative effects. The study is based on multiannual simulations with the Chemical Lagrangian Model of the Stratosphere (CLaMS) driven by ERA-Interim meteorological data and on a state-of-the-art radiance code. Mixing, the irreversible part of transport, is controlled by the local horizontal strain and vertical shear of the atmospheric flow. We find that simulated radiative effects of water vapor and ozone, both characterized by steep gradients in the UTLS, are particularly sensitive to uncertainties of the atmospheric mixing strength. Globally averaged radiative effects are about 0.72 and 0.17 W/m$^2$ for water vapor and ozone, respectively. For ozone, the largest impact of mixing uncertainties is observed in the extra-tropical lower stratosphere.

**Citation:** Riese, M., F. Ploeger, A. Rap, B. Vogel, P. Konopka, M. Dameris, and P. Forster (2012), Impact of uncertainties in atmospheric mixing on simulated UTLS composition and related radiative effects, *J. Geophys. Res.*, *117*, D16305, doi:10.1029/2012JD017751.

## 1. Introduction

[2] The atmospheric region of the upper troposphere/lower stratosphere (UTLS) plays a crucial role in the climate system. Changes in temperature as well as in distributions and concentrations of radiatively active gases in the UTLS result in particularly large changes in radiative forcings, which trigger climate change [*Intergovernmental Panel on Climate Change*, 2007]. In spite of its immense significance, the UTLS is one of the least understood regions of the atmosphere. This is a result of its great dynamic, microphysical and chemical complexity. Projections of future climate change are therefore subject to uncertainties in model representations of UTLS temperature and chemical composition and their changes in a changing climate.

[3] Multimodel intercomparisons show significant differences in UTLS concentrations of water vapor and ozone, two important greenhouse gases, with global distributions mainly depending on the details of the presentation of underlying processes [e.g., *Gettelman et al.*, 2010; *Hegglin et al.*, 2010; *SPARC CCMVal*, 2010]. *Stevenson et al.* [2006] point to large model differences in the representation of stratosphere-troposphere exchange (STE) that result in considerable uncertainties in the simulated ozone budget, in particular in the upper troposphere. *Solomon et al.* [2010] highlight that global models are rather limited in their representation of key processes determining the distribution and variability of lower stratospheric water vapor. Consequently, observed long-term variations of water vapor in this region are not adequately reproduced by these models, although they represent an important driver of climate change on decadal timescales.

[4] In this paper, we assess the influence of current uncertainties in the atmospheric mixing strength on global UTLS distributions of greenhouse gases (water vapor, ozone, methane, and nitrous oxide) and associated radiative effects. The study is based on multiannual simulations with the Lagrangian CLaMS model [*McKenna et al.*, 2002a, 2002b; *Konopka et al.*, 2010, and references therein] driven by ECMWF ERA-Interim meteorological data [*Simmons et al.*, 2006].

[5] Atmospheric mixing, the irreversible part of transport, is controlled by a critical deformation of the flow $\gamma_c$ (expressed as critical Lyapunov coefficient $\lambda_c$). A brief description of this concept and the deduction of the critical mixing parameter $\lambda_c$ is given in Section 3.1. In order to assess the sensitivity of the simulation results on uncertainties in the atmospheric mixing strength, $\lambda_c$ is varied within current uncertainty limits. The impact of associated trace gas

[1]Institute of Energy and Climate Research, Stratosphere, Forschungszentrum Jülich, Jülich, Germany.
[2]School of Earth and Environment, University of Leeds, Leeds, UK.
[3]Deutsches Zentrum für Luft- und Raumfahrt, Institut für Physik der Atmosphäre, Oberpfaffenhofen, Germany.

Corresponding author: M. Riese, Institute of Energy and Climate Research, Stratosphere, Forschungszentrum Julich GmbH IEK-7 52425 Julich Germany. (M.Riese@fz-juelich.de)


0148-0227/12/2012JD017751

variations on the radiative effects of important greenhouse gases (water vapor, ozone, methane, and nitrous oxide) is calculated using a state-of-the-art radiation scheme [*Edwards and Slingo*, 1996].

[6] In Section 2, we demonstrate the large sensitivity of surface temperature to composition changes in the UTLS. The composition of the UTLS is, in turn, governed by rather complex processes such as stratosphere-troposphere exchange (STE). Section 3 gives a description of the CLaMS model and the setup used for our simulations. The sensitivity of simulated concentrations and spatial distributions of water vapor, ozone, methane, and nitrous oxide to uncertainties of the atmospheric mixing strength is described in Section 4. The results are interpreted in terms of the radiative effect (differences in radiative fluxes) of the uncertainty of atmospheric mixing strength. Section 5 gives a brief summary and discussion.

## 2. The Role of the UTLS for Radiative Forcings

### 2.1. Sensitivity of Surface Climate to UTLS Composition

[7] The upper troposphere/lower stratosphere (UTLS) refers to the region in the atmosphere that spans a height interval from about 6 to 25 km including the cold tropopause. The UTLS is a region of rather low temperatures and plays an important role for atmospheric cooling to space and radiative forcings of the atmosphere. The radiation balance of the UTLS is predominantly controlled by temperature, spatially highly variable concentrations of greenhouse gases such as water vapor and ozone, and well-mixed greenhouse gases such as carbon dioxide ($CO_2$), methane ($CH_4$), nitrous oxide ($N_2O$), chlorofluorocarbons (CFCs), and ice clouds (cirrus). Even small changes of temperature, greenhouse gases, and the abundance of cloud particles can have a significant impact on atmospheric radiative forcings [e.g., *Forster and Shine*, 1997, 2002; *Zhang et al.*, 2004]. Consequently, surface climate exhibits a large sensitivity to temperature and composition changes in the UTLS.

[8] In general, the height-integrated radiative forcing of surface temperature for changes in the vertical distribution of trace gases can be obtained by integrating a height-dependent sensitivity function (or weighting function) with height-dependent changes in the vertical trace gas concentration [e.g., *Lacis et al.*, 1990; *Solomon et al.*, 2010].

[9] Figure 1 shows 2D sensitivity functions (altitude x latitude grid) calculated for ozone (Figure 1, left), water vapor (Figure 1, middle), and methane (Figure 1, right) on the basis of a reference atmosphere constructed from ECMWF reanalysis data [see *Rap et al.*, 2010]. The values shown in Figure 1 were obtained by calculating the radiative effects of trace gas perturbations (increases) at all grid points individually, leaving concentrations at other grid points unchanged. Trace gas values of the reference atmosphere were modified either by fixed unit mass (Figure 1, top) or by 1% increases (Figure 1, bottom). Figure 1 shows radiative effects that have been normalized for each trace gas to the maximum value obtained. The resulting 2D sensitivity functions highlight the importance of trace gas changes in the UTLS for surface climate. These 2D sensitivity functions represent a challenge for climate projections, because the spatial distributions (and changes) of important greenhouse gases in the UTLS result from complex interactions of numerous atmospheric processes that operate at different spatial and temporal scales. Stratosphere-troposphere exchange (STE) plays a dominant role in this context. Simulations of STE, in turn, crucially depend on the advection and mixing schemes used by models. Before coming back to this in Section 4, we give a brief overview of current knowledge of the complexity of STE and its underlying transport and microphysical processes.

### 2.2. Variability of UTLS Composition Resulting From STE

[10] Important greenhouse gases such as water vapor and ozone, with steep gradients between their tropospheric and stratospheric mixing ratio values, exhibit large spatial and temporal variability in the UTLS as a result of stratosphere-troposphere exchange. Prominent underlying processes are the Brewer-Dobson circulation, quasi-horizontal isentropic transport between the tropical tropopause layer (TTL) and the extra-tropical lowermost stratosphere (LMS), and vertical transport from below by convection.

[11] Transport of air from the troposphere deep into the stratosphere occurs mainly in the tropics and is associated with the ascending branch of the large-scale Brewer-Dobson circulation, which connects the tropical tropopause layer (TTL) [see *Fueglistaler et al.*, 2009] with the deep stratosphere. The tropical upwelling of air is balanced by poleward transport and net downwelling (timescale of years) in the extra-tropics. There is also evidence for a fast (shallow) component of the Brewer-Dobson circulation [e.g., *Birner and Boenisch*, 2011; *Garny et al.*, 2011] that connects the tropics with the subtropics in a more direct manner.

[12] Global observations of HCN, a pollutant produced by biomass burning, indicate that during the northern hemispheric summer the Asian monsoon circulation provides an important pathway for air masses from the troposphere into the ascending branch of the Brewer-Dobson circulation in the lower stratosphere [*Randel et al.*, 2010]. Another prominent feature of the Asian monsoon circulation in terms of stratosphere-troposphere exchange is the presence of an anticyclone located in the upper troposphere extending from Asia to the Middle East. At the edge of this anticyclone, extra-tropical stratospheric air is transported equatorwards, significantly affecting trace gas budgets (e. g., ozone) in the upper part of the TTL [e.g., *Konopka et al.*, 2010].

[13] Bi-directional quasi-horizontal transport of air across the edges of the subtropical jet plays an important role in connecting the tropical troposphere (including the TTL) with the extra-tropical lowermost stratosphere. The quasi-horizontal transport between the upper TTL in the tropics and the lowermost stratosphere in the extra-tropics is triggered by disturbances of the subtropical jet by Rossby waves (timescales of days to weeks). A prominent feature in the extra-tropical UTLS is the extra-tropical transition layer (ExTL), a region in the vicinity of the tropopause that is strongly influenced by stratosphere-troposphere exchange. A comprehensive overview of the various transport processes governing the composition of the extra-tropical UTLS is given in the review paper by *Gettelman et al.* [2011].

### 2.3. Challenges in Modeling UTLS Composition

[14] It is a challenging task to model all the complex transport processes described in the previous subsection as well as their spatial and temporal variability. Steep trace gas

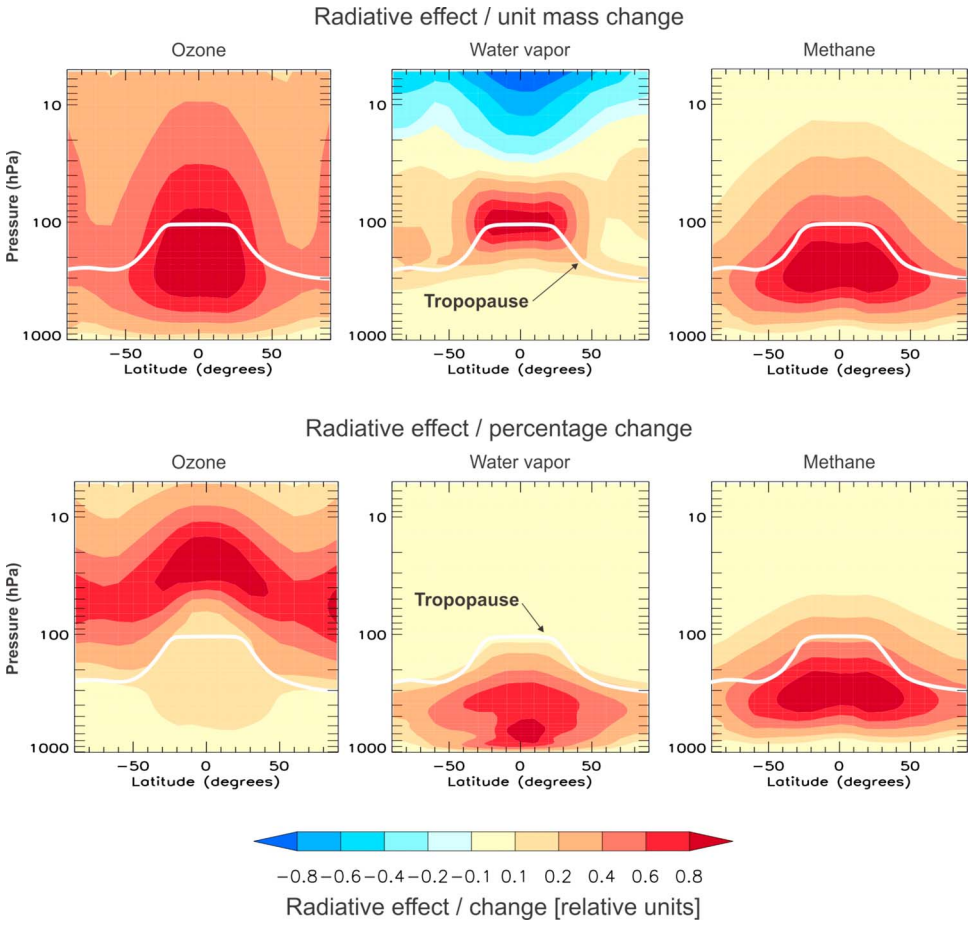


**Figure 1.** Sensitivity of surface temperature to the altitude and latitude of (left) ozone, (middle) water vapor, and (right) methane changes. Shading shows relative impact on surface temperature, measured as radiative effect, from either (top) unit mass increases or (bottom) percentage increases applied at individual latitudes and altitudes (1 km thick layers). For each trace gas, the calculated radiative effects have been normalized to the respective maximum value. Red tones are indicative of warming, blue tones indicate cooling. The figure shows, for example, that the impact on surface temperature of an ozone unit mass change at 100 hPa at the equator is about a factor of 2 larger than the impact of the same change at 10 hPa. The figure follows a methodology outlined by *Forster and Shine* [1997].

gradients and small-scale filamentary structures play an important role in the transport processes sketched above. Reliable transport schemes therefore represent a prerequisite for a quantitative representation of important greenhouse substances in the UTLS.

[15] *Stenke et al.* [2008] demonstrated that an unrealistic water vapor distribution in the UTLS region (e.g., insufficient representation of the strong vertical gradient with high mixing ratios in the troposphere and low mixing ratios in the stratosphere) is to a large extent responsible for the cold bias in the polar tropopause region and the cold pole problem in the polar lower stratosphere, a feature which is found in many atmospheric general circulation models (AGCMs) and chemistry climate models (CCMs). *Ploeger et al.* [2010, 2011] highlighted the large sensitivity of UTLS composition (ozone and water vapor) to uncertainties in the representation of vertical advection by using a backward trajectory model driven by ERA-Interim meteorological data.

[16] In addition to uncertainties in advection, all Lagrangian and Eulerian transport schemes are subject to uncertainty concerning the influence of mixing, the irreversible part of transport. The influence of this uncertainty is investigated below on the basis of the Lagrangian model CLaMS, which contains a physically based adjustable parameterization of the atmospheric mixing strength.

## 3. Simulations

### 3.1. Mixing Concept of CLaMS

[17] The Chemical Lagrangian Model of the Stratosphere (CLaMS) is the first chemistry transport model (CTM) with a Lagrangian transport scheme where the concept of mixing based on the atmospheric flow deformation has been successfully realized [*McKenna et al.*, 2002a, 2002b; *Konopka et al.*, 2004]. In regions of strong flow deformations, such as the subtropical jets, strong mixing occurs [*Pan et al.*, 2006; *Konopka et al.*, 2007; *Vogel et al.*, 2011], while in regions of weak flow deformations, mixing is also weak. CLaMS was originally developed for the stratosphere and recently extended to the troposphere [*Konopka et al.*, 2007, 2010].


**Figure 2.** Deformation of a small circle with radius $r_0$ in the atmospheric flow. For sufficiently small values of $r_0$ and time steps $\Delta t$ the resulting deformation can be approximated by an ellipse with minor and major axes $r_-$ and $r_+$. For an incompressible flow both the elongation and the contraction rates of the ellipse can be expressed in terms of a single Lyapunov exponent $\lambda$, i.e., $r_-/r_0 = \exp(-\lambda \cdot \Delta t)$ and $r_+/r_0 = \exp(+\lambda \cdot \Delta t)$.

The model is well known for representing transport and mixing processes in the UTLS quite realistically. This has been shown by numerous intercomparisons of model results with measurements in the tropics and extra-tropics and for various seasons [e.g., *Konopka et al.*, 2007; *Grooß et al.*, 2008; *Günther et al.*, 2008; *Vogel et al.*, 2011].

[18] The concept of deformation-induced mixing is motivated by the characteristics of stratospheric transport, where the large-scale horizontal flow gives rise to chaotic advection of tracers [*Lorenz*, 1963]. A prominent feature of this advection is the occurrence of pronounced streamers and filaments that have also been observed, for example, by high-resolution satellite observations [e.g., *Riese et al.*, 1999, 2002]. Dissipation of these structures is associated with a scale collapse, which occurs in regions with strong shear rates. The Lagrangian approach is well suited for resolving small-scale structures such as elongated filaments associated with the scale collapse down to rather fine scales (a few tens of km in the case of CLaMS).

[19] The concept of deformation-induced mixing was successfully realized in CLaMS both in two and three dimensions [*McKenna et al.*, 2002a; *Konopka et al.*, 2004]. Unlike Eulerian transport models, CLaMS considers an ensemble of air parcels on a time-dependent irregular grid with an initial horizontal air parcel separation $r_0$ (here 100 km). Each transport step (here 24 h) consists of two parts: pure advection based on trajectory calculations ($\Delta t$ = 1 h) and a subsequent calculation of mixing effects. During the advection step, parts of the grid undergo deformation caused by horizontal strain in the 2D (isentropic) version or by the coupled horizontal strain and vertical shear in the 3D version of CLaMS. In an incompressible flow, this deformation can be quantified by only one parameter $\gamma$ measuring the eccentricity of an ellipse as illustrated in Figure 2. The deformation of the grid allows the scale collapse to be resolved down to $r_0 \cdot \exp(-\gamma)$. If the deformation parameter $\gamma$ exceeds a prescribed critical value $\gamma_c$, the grid is reordered by insertion or merging of air parcels, which leads to mixing. By this approach, the integral effect of mixing, which is the final step of the scale collapse, is coupled to the integral deformations in the flow over the time step of transport. The critical deformation parameter $\gamma_c$ can also be expressed in terms of a critical Lyapunov exponent $\lambda_c$ with $\gamma_c = \lambda_c \cdot \Delta t$.

[20] The first choice and validation of the deformation parameter for the 2D version of CLaMS was based on a qualitative reproduction of structures in stratospheric $N_2O$ fields observed by the CRISTA satellite instrument in early November 1994 [*Offermann et al.*, 1999; *McKenna et al.*, 2002a]. *Konopka et al.* [2005] refined this analysis by employing the probability density function (PDF) technique [e.g., *Sparling*, 2000] and found a lower limit for the critical deformation $\gamma_c$ of 0.8 ($\lambda_c$ = 0.8 day$^{-1}$, $\Delta t$ = 24 h). This result turned out to be very robust with respect to different transport time steps (6 to 24 h) and different resolutions of the initial grid (e.g. 100 km and 200 km). *Khosrawi et al.* [2005] simulated PDFs for the CRISTA case using critical deformations of 0.75 and 1.2 and found rather small differences compared to differences with PDFs obtained from the Eulerian KASIMA (T106) model, which underestimates the strength of the observed tracer structures.

[21] CRISTA observations of $N_2O$ are characterized by a comparatively high spatial resolution for a satellite instrument of about 200 km horizontally and 2.5 km vertically. However, smoothing of atmospheric structures such as fine filaments by the instrument averaging kernels decreases the width of PDFs and results in an underestimation of the critical deformation rate. The 2D mixing scheme of CLaMS was therefore also applied to the analysis of filamentary structures in both long-lived (CH4, halon-1211) and chemically active species ($ClONO_2$, and NO) measured (in situ) onboard the ER-2 during flights across filaments near the edge of the polar vortex in March 2000. These studies focused on the reproduction of observed correlations, in addition to the structure and variability of single tracers. *Konopka et al.* [2003] found the best consistency between observations and simulations for a critical deformation $\gamma_c$ around 1.2 ($\lambda_c$ = 1.2 day$^{-1}$, $\Delta t$ = 24 h).

[22] For the 3D version, the observed correlations could be best reproduced for values of the critical deformation $\gamma_c$ between 1.0 and 1.5 ($\lambda_c$ = 1.5 day$^{-1}$; $\Delta t$ = 24 h) and a horizontal grid resolution between 100 and 200 km [*Konopka et al.*, 2004]. Using a critical deformation of $\gamma_c$ = 1.5 ($\lambda_c$ = 1.5 day$^{-1}$; $\Delta t$ = 24 h), *Konopka et al.* [2007] studied transport across the tropical tropopause layer (TTL) and obtained a good correspondence between trace gas structures measured (in situ) on board the Geophysica aircraft over Brazil and corresponding CLaMS simulations. *Grooß et al.*, 2005, 2008] used a somewhat lower critical deformation of $\gamma_c$ = 1.2 ($\lambda_c$ = 1.2 day$^{-1}$; $\Delta t$ = 24 h) for studies of ozone loss processes in the Arctic winter stratosphere based on (in situ) observations on board Geophysica and found good agreement between observed and simulated tracer structures (e.g., for $N_2O$ as well. Finally, a recent study [*European Space Agency*, 2012] indicates that fine filamentary mixing structures

of polar air from midlatitudes, remotely observed by infrared limb-sounding from the research aircraft Geophysica, are well reproduced by CLaMS simulations using deformation rates $\gamma_c$ of 1.2 and 1.5, with a slightly better agreement for the higher value. The study also indicates that current uncertainties in the atmospheric mixing strength could be significantly reduced by global observations employing the infrared limb-imaging technique [*Riese et al.*, 2005] that provides three-dimensional observations of high spatial resolution (0.75 km vertically; few tens of km horizontally) for a large number of atmospheric species including water vapor and ozone.

[23] While the remaining uncertainties of the Lyapunov coefficients were not so critical for previous studies focusing on episodes or mixing events, we show in Section 4 that they have a significant impact on simulated background fields of water vapor and ozone in the tropopause region in multi-annual simulations.

### 3.2. ClaMS Setup

[24] For the simulations discussed in this paper, we used ERA-Interim reanalysis data for the trajectory calculation (advective part of transport). The vertical velocity above an altitude of about 300 hPa, the region of interest here, is deduced from the ERA-Interim forecast total diabatic heating rate, including the effects of all-sky radiative heating, latent heat release and diffusive heating as described in *Ploeger et al.* [2010]. Below this altitude, the vertical model coordinate smoothly transforms into an orography-following $\sigma$-coordinate, with the vertical velocity transforming into the corresponding $\dot{\sigma}$ [*Mahowald et al.*, 2002].

[25] We carried out two CLaMS simulations with different values of the critical Lyapunov exponent $\lambda_c$ (1.5 day$^{-1}$ and 1.2 day$^{-1}$, see Section 4) to study the influence of mixing on the distribution of the most relevant species ($O_3$, $H_2O$, $N_2O$, $CH_4$) in the vicinity of the tropopause. These global CLaMS simulations cover the time period from 1 October 2001 to 31 December 2003 and cover both the troposphere and the stratosphere. The horizontal air parcel separation is around 100 km in this case. The vertical resolution at the tropical tropopause is adapted via an aspect ratio $\alpha$ = 250 [*Haynes and Anglade*, 1997], expressing the ratio between horizontal and vertical scales [*Konopka et al.*, 2007]. This results in a vertical resolution of about 400 m around the tropopause. Initial trace gas concentrations are prescribed from observational and model data at the lower model boundary. Water vapor values in the lower troposphere are prescribed by ECMWF. Freeze drying of water vapor (dehydration) is calculated based on a simplified cirrus treatment with a one hour time step. Freeze drying occurs as soon as the relative humidity exceeds 100%. Ice sedimentation is included in the dehydration scheme, based on the fall velocity of (spherical) ice particles [*von Hobe et al.*, 2011].

### 3.3. Radiation Code

[26] The radiation model used is from *Edwards and Slingo* [1996], in the off-line version. The version used here employs 6 bands in the shortwave and 9 bands in the longwave and adopts a delta-Eddington 2 stream scattering solver at all wavelengths. This radiation model uses as its input monthly mean climatological cloud fields and surface albedo (averaged over the period from 1983 to 2005) from the International Satellite Cloud Climatology Project (ISCCP) [*Rossow and Schiffer*, 1999]. Clouds are added to three unique vertical levels corresponding to low, middle and high clouds. The standard climatological water vapor, temperature and trace gas data are based on ECMWF reanalysis data (for details, see *Rap et al.* [2010]). This variant of the radiation code has been extensively tested against line-by-line models in *Forster et al.* [2011], and was found to agree very well (better than 10% in the net forcing) for estimating forcing changes in tropospheric water vapor, tropospheric ozone and methane.

## 4. Simulation Results

[27] The radiative effects of uncertainties in atmospheric mixing strength are calculated by a two-step approach. First, the sensitivity of the simulated UTLS trace-gas distribution to uncertainties in the atmospheric mixing strength is determined. The resulting differences of trace gas concentrations are then converted into radiative effects in order to access the potential impact on climate projections.

[28] To determine the sensitivity of the trace gas fields to the mixing strength, we made two simulations that only differ in the value of the mixing parameter $\lambda_c$ (critical Lyapunov exponent), 'a reference simulation' with a value of $\lambda_c$ = 1.5 day$^{-1}$ and an 'enhanced mixing simulation' with a value of $\lambda_c$ = 1.2 day$^{-1}$. These particular values of the mixing parameter $\lambda_c$ appear to be well inside the current uncertainty range for mixing induced by flow-deformation as discussed in Section 3.1. In the upper troposphere, the decreased static stability and the influence of unresolved convection add an additional dimension to the uncertainties in the representation of mixing in global atmospheric models.

[29] Figure 3 shows zonally averaged fields from the reference run for water vapor, ozone, nitrous oxide, and methane, respectively. The simulated fields resemble the main spatial structures found in climatologies obtained from satellite observations [cf. e.g., *Grooß and Russell*, 2005]. Figure 4 shows mixing ratio differences for the trace gases obtained from the reference simulation and respective values from the enhanced mixing simulation. Figure 5 shows the same but for percentage differences. The largest differences occur in the vicinity of the largest spatial gradients of the respective trace gases.

[30] As a result of enhanced mixing, an increase of water vapor concentrations in the extra-tropical lowermost stratosphere of 10 to 15% is found. This increase can mainly be attributed to differences in the quasi-horizontal (isentropic) transport of air masses from the upper tropical troposphere into the extra-tropical lowermost stratosphere, a process that is well captured by CLaMS. In terms of mixing ratio values, the largest differences for water vapor occur in the upper tropical troposphere. As mentioned above, these differences only reflect part of the mixing uncertainty, because the influence of unresolved convective effects may be rather large in the tropical upper troposphere.

[31] For ozone, enhanced mixing results in a significant increase in mixing ratios at the transition of the tropical to the extra-tropical tropopause (about 30%) and throughout the lower stratosphere. The altitudes of the largest increases coincide with the altitudes where changes have the largest impact on surface temperature (compare Figure 1).

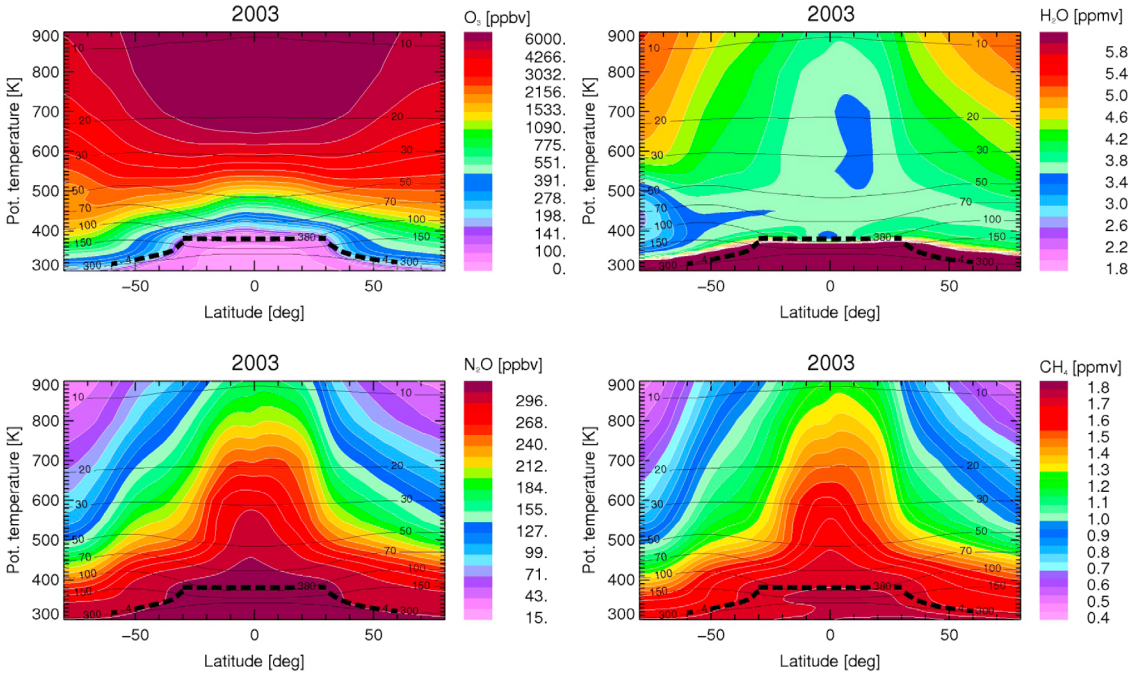


**Figure 3.** Zonally averaged trace gas values from the CLaMS reference run for 2003: (top left) ozone, (top right) water vapor, (bottom left) nitrous oxide, and (bottom right) methane. Potential temperature ($\Theta$) is used as vertical coordinate. Pressure levels are also shown by thin black lines.

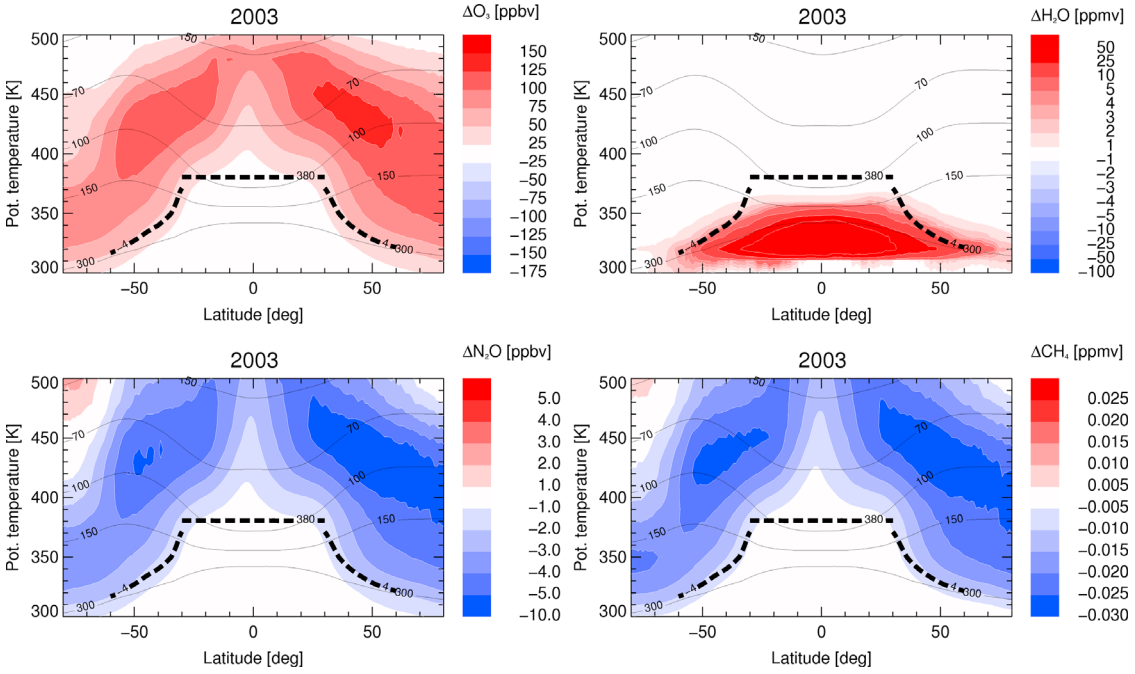


**Figure 4.** Difference in trace gas mixing ratios between the enhanced mixing run ($\lambda = 1.2$ day$^{-1}$, see text) and the reference run ($\lambda = 1.5$ day$^{-1}$) for 2003: (top left) ozone, (top right) water vapor, (bottom left) nitrous oxide, (bottom right) methane. Shown are zonally averaged annual mean (2003) differences in concentrations. Potential temperature ($\Theta$) is used as vertical coordinate. Pressure levels are also shown by thin black lines.

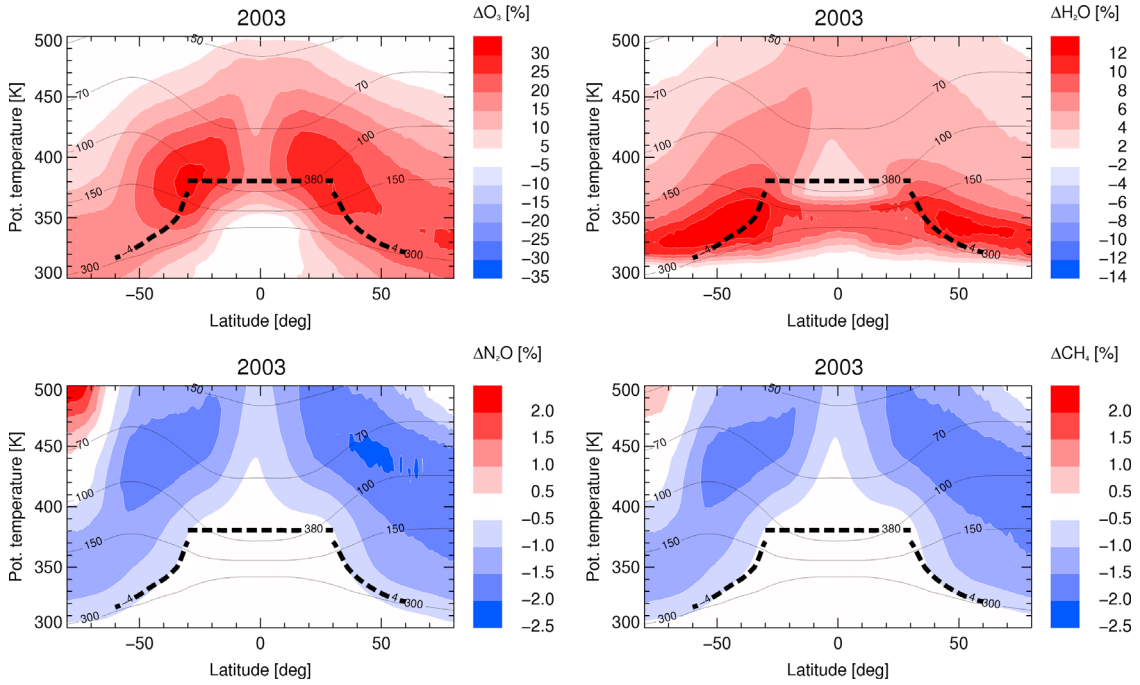


**Figure 5.** Percentage difference in trace gas concentrations between the enhanced mixing run ($\lambda$ = 1.2 day$^{-1}$, see text) and the reference run ($\lambda$ = 1.5 day$^{-1}$) for 2003: (top left) ozone, (top right) water vapor, (bottom left) nitrous oxide, and (bottom right) methane. Shown are zonally averaged annual mean (2003) differences in percentage values. Potential temperature ($\Theta$) is used as vertical coordinate. Pressure levels are also shown by thin black lines.

[32] The corresponding annual mean radiative effects of this change in the atmospheric mixing strength are shown in Figure 6. These radiative effects were calculated from horizontally and vertically resolved monthly mean trace gas distributions. [*Rap et al.*, 2010] found for contrails a correlation between areas of contrail forcing and high cloud cover that necessitated the use of 6 hourly data in the forcing calculation. In our case, there is, however, very little correlation between water vapor forcing and high cloud cover, allowing us to employ monthly data for the calculation of the water vapor forcing.

[33] Figure 6 illustrates that the radiative effects of water vapor and ozone, both with steep gradients in the UTLS, are very sensitive to uncertainties in the mixing. For water vapor, the largest radiative effect is found at equatorial latitudes with values reaching about 1.5 W/m$^2$. The globally averaged effect for water vapor at the top-of-the-atmosphere (TOA) is 0.72 W/m$^2$. The global distribution of the radiative effects resembles the mixing ratio differences shown in Figure 4, highlighting the large contribution of changes in the tropical upper troposphere. The increase of the water vapor concentration in the upper tropical troposphere in the enhanced mixing case will also modify the formation and microphysics of clouds and thus the radiative effects of clouds. An analysis of this highly uncertain contribution is, however, beyond the scope of our study.

[34] For ozone, the radiative effects are also found to be surprisingly large, reaching values of up to about 0.40 W/m$^2$ at middle and high northern latitudes. The global mean TOA radiative effect is 0.17 W/m$^2$. The largest contribution to the radiative effect of ozone is provided by the lower stratosphere, highlighting the importance of a quantitative understanding of processes in the lower stratosphere for a quantitative representation of the ozone forcing.

[35] In contrast to $H_2O$ and $O_3$, simulated radiative effects of $N_2O$, and $CH_4$, both relatively well mixed, turn out to be rather insensitive. Global mean TOA radiative effects for these two gases amount only to about $-2$ mW/m$^2$ and $-0.5$ mW/m$^2$, respectively.

## 5. Summary and Discussion

[36] The representation of composition changes in the UTLS in climate prediction generally involves two major sources of uncertainty. The first is the definition of emission scenarios for anthropogenic greenhouse gases such as carbon dioxide and methane. The second is the representation of physical and chemical processes that affect the composition of the UTLS. An adequate representation of natural greenhouse gases such as water vapor and ozone, which exhibit large spatial gradients in the UTLS, relies on a realistic representation of transport in the atmosphere (e.g., stratosphere-troposphere exchange). The underlying transport can be divided into two parts: (1) advection caused by horizontal and vertical winds and (2) mixing, the irreversible part of transport. While the influence of inadequate advection schemes has received some attention in the past [e.g., *Stenke et al.*, 2008; *Ploeger et al.*, 2010], the impact of atmospheric mixing has not yet been evaluated.

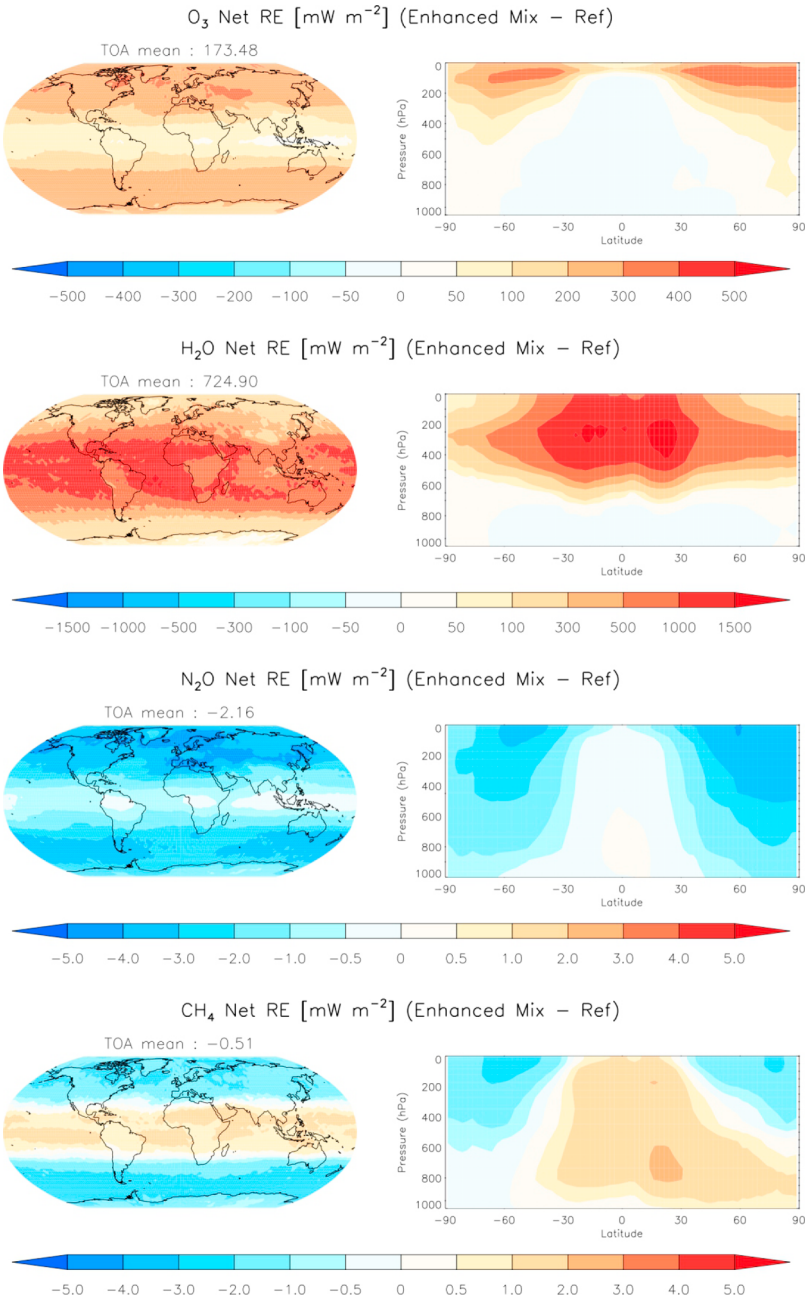


**Figure 6.** Radiative effects of the enhanced mixing simulation (compared to the reference simulation) for ozone, water vapor, nitrous oxide and methane (left) at the TOA and (right) zonally averaged. The numerical values given above the left panels are TOA annual global means for 2003.

[37] We used the Lagrangian model CLaMS to study the impact of uncertainties in the atmospheric mixing strength on climate projections. In this model the degree of mixing can be controlled by a critical Lyapunov coefficient $\lambda_c$. The model has a particular strength in simulating transport and mixing effects in the vicinity of transport barriers (e.g., polar and sub-tropical jets) that are characterized by strong wind shear and large spatial gradients in a number of important greenhouse gases [e.g., *Konopka et al.*, 2007; *Vogel et al.*, 2011]. It is therefore also well suited for assessing the impact of uncertainties in the atmospheric mixing strength on climatological distributions of important greenhouse gases such as water vapor, ozone, $CH_4$, and $N_2O$ in this region of the atmosphere.

[38] We determined this impact and associated radiative effects. For water vapor and ozone, annual mean globally averaged TOA radiative effects of 0.72 and 0.17 W/m$^2$ are found, respectively. For comparison, changes of the radiative forcing since 1980 due to well-mixed greenhouse gases, aerosols, and stratospheric water vapor are of the order of 1.0 W/m$^2$ [*Solomon et al.*, 2010]. *Solomon et al.* [2010] derived the impact of this radiative forcing change on

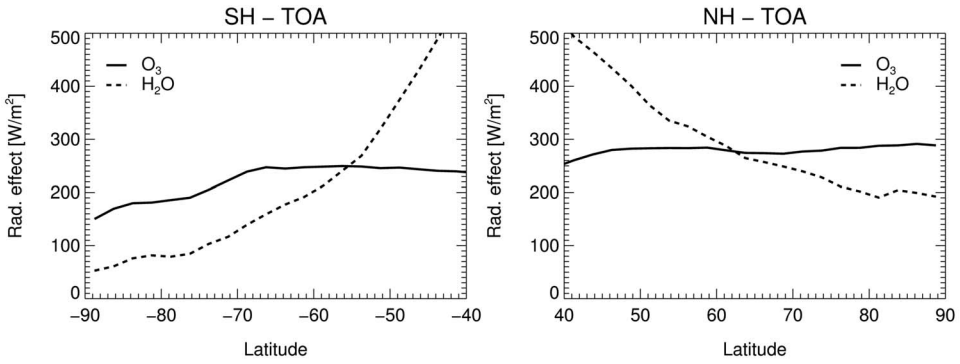


**Figure 7.** Radiative effects (TOA) of the enhanced mixing simulation compared to the reference simulation for ozone and water vapor at middle and high latitudes. Shown are zonal mean values for 2003. (left) Values for the southern hemisphere (SH) and (right) values for the northern hemisphere (NH).

global surface temperature and found a value of about 0.4 K. The climate sensitivity of the model used for this assessment was 3 K for a doubling of atmospheric $CO_2$.

[39] For ozone, the radiative effect of mixing uncertainties mainly results from changes in the stratosphere. The effect is as large as about 40% of the total anthropogenic tropospheric ozone forcing [*Intergovernmental Panel on Climate Change*, 2007]. The radiative effect of stratospheric ozone due to mixing uncertainties is the most reliable result of our simulations, because transport and mixing in the stratosphere are particularly well represented in CLaMS and changes in ozone are not correlated with changes in clouds. Figure 7 indicates that the simulated radiative forcing effects of ozone are on average about equally important as water vapor effects at middle and higher latitudes. The relative importance of simulated ozone effects increases from middle to higher latitudes.

[40] The radiative effects for water vapor and ozone are relatively high compared to the effects simulated for methane and nitrous oxide. This is mainly a result of the extremely steep mixing ratio gradients of water vapor and ozone in the UTLS and the corresponding sensitivity to uncertainties in transport schemes. Ozone values are particularly sensitive to mixing uncertainties in the lower stratosphere. At the same time, ozone changes in the lower stratosphere have the largest impact on the ozone radiative forcing (see Figure 1). This finding highlights the importance of a quantitative understanding of mixing processes in this region of the atmosphere.

[41] **Acknowledgments.** The work presented here was partly funded by the European Space Agency (ESA) as part of the project "PREMIER - Quantification of Atmospheric Pollution and Climate Aspects" under Request for Quotation AO/1-6340/09/NL/CBi. We sincerely thank the responsible ESA officer, Jörg Langen, and the whole study team for very fruitful discussions. The work of Alexandru Rap was supported by the UK NERC grant NE/G005109/1.

## References

Birner, T., and H. Boenisch (2011), Residual circulation trajectories and transit times into the extratropical lowermost stratosphere, *Atmos. Chem. Phys.*, *11*(2), 817–827, doi:10.5194/acp-11-817-2011.

Edwards, J., and A. Slingo (1996), Studies with a flexible new radiation code: 1. Choosing a configuration for a large-scale model, *Q. J. R. Meteorol. Soc.*, *122*, 689–719.

European Space Agency (2012), Report for mission selection: PREMIER, *Eur. Space Agency Spec. Publ.*, *ESA SP-1324/3*, 234 pp.

Forster, P., and K. P. Shine (1997), Radiative forcing and temperature trends from stratospheric ozone changes, *J. Geophys. Res.*, *102*(D9), 10,841–10,855, doi:10.1029/96JD03510.

Forster, P., and K. P. Shine (2002), Assessing the climate impact of trends in stratospheric water vapor, *Geophys. Res. Lett.*, *29*(6), 1086, doi:10.1029/2001GL013909.

Forster, P. M., et al. (2011), Evaluation of radiation scheme performance within chemistry climate models, *J. Geophys. Res.*, *116*, D10302, doi:10.1029/2010JD015361.

Fueglistaler, S., A. E. Dessler, T. J. Dunkerton, I. Folkins, Q. Fu, and P. W. Mote (2009), Tropical tropopause layer, *Rev. Geophys.*, *47*, RG1004, doi:10.1029/2008RG000267.

Garny, H., M. Dameris, W. Randel, G. E. Bodeker, and R. Deckert (2011), Dynamically forced increase of tropical upwelling in the lower stratosphere, *J. Atmos. Sci.*, *68*, 1214–1233, doi:10.1175/2011JAS3701.1.

Gettelman, A., et al. (2010), Multi-model assessment of the upper troposphere and lower stratosphere: Tropics and global trends, *J. Geophys. Res.*, *115*, D00M08, doi:10.1029/2009JD013638.

Gettelman, A., P. Hoor, L. L. Pan, W. J. Randel, M. I. Hegglin, and T. Birner (2011), The extratropical upper troposphere and lower stratosphere, *Rev. Geophys.*, *49*, RG3003, doi:10.1029/2011RG000355.

Grooß, J.-U., and J. Russell III (2005), Technical note: A stratospheric climatology for $O_3$, $H_2O$, $CH_4$, NOx, HCl and HF derived from HALOE measurements, *Atmos. Chem. Phys.*, *5*, 2797–2807.

Grooß, J. U., G. Günther, R. Müller, P. Konopka, S. Bausch, H. Schlager, C. Voigt, C. M. Volk, and G. C. Toon (2005), Simulation of denitrification and ozone loss for the Arctic winter 2002/2003, *Atmos. Chem. Phys.*, *5*, 1437–1448.

Grooß, J.-U., R. Müller, P. Konopka, H.-M. Steinhorst, A. Engel, T. Möbius, and C. M. Volk (2008), The impact of transport across the polar vortex edge on Match ozone loss estimates, *Atmos. Chem. Phys.*, *8*, 565–578.

Günther, G., R. Müller, M. von Hobe, F. Stroh, P. Konopka, and C. M. Volk (2008), Quantification of transport across the boundary of the lower stratospheric vortex during Arctic winter 2002/2003, *Atmos. Chem. Phys.*, *8*(13), 3655–3670.

Haynes, P., and J. Anglade (1997), The vertical scale cascade in atmospheric tracers due to large-scale differential advection, *J. Atmos. Sci.*, *54*, 1121–1136.

Hegglin, M. I., et al. (2010), Multi-model assessment of the upper troposphere and lower stratosphere: Extra-tropics, *J. Geophys. Res.*, *115*, D00M09, doi:10.1029/2010JD013884.

Intergovernmental Panel on Climate Change (2007), *Climate Change 2007: The Physical Science Basis. Contribution of Working Group I to the Fourth Assessment Report of the Intergovernmental Panel on Climate Change*, edited by S. Solomon et al., 996 pp., Cambridge Univ. Press, Cambridge, U. K.

Khosrawi, F., J.-U. Grooß, R. Müller, P. Konopka, W. Kouker, R. Ruhnke, T. Reddmann, and M. Riese (2005), Intercomparison between Lagrangian and Eulerian simulation of the development of mid-latitude streamers as observed by CRISTA, *Atmos. Chem. Phys.*, *5*, 85–95.

Konopka, P., J. U. Grooß, G. Günther, D. S. McKenna, R. Müller, J. W. Elkins, D. Fahey, and P. Popp (2003), Weak impact of mixing on chlorine deactivation during SOLVE/THESEO 2000: Lagrangian modeling (CLaMS) versus ER-2 in situ observations, *J. Geophys. Res.*, *108*(D5), 8324, doi:10.1029/2001JD000876.

Konopka, P., et al. (2004), Mixing and ozone loss in the 1999–2000 Arctic vortex: Simulations with the 3-dimensional Chemical Lagrangian Model of the Stratosphere (CLaMS), *J. Geophys. Res.*, *109*, D02315, doi:10.1029/2003JD003792.

Konopka, P., G. Günther, D. S. McKenna, R. Müller, D. Offermann, R. Spang, and M. Riese (2005), How homogeneous and isotropic is stratospheric mixing? Comparison of CRISTA-1 observations with transport studies based on the Chemical Lagrangian Model of the Stratosphere (CLaMS), *Q. J. R. Meteorol. Soc.*, *131*(606), 565–579, doi:10.1256/qj.04.47.

Konopka, P., et al. (2007), Contribution of mixing to upward transport across the tropical tropopause layer (TTL), *Atmos. Chem. Phys.*, *7*(12), 3285–3308.

Konopka, P., J.-U. Grooß, G. Günther, F. Plöger, R. Pommrich, R. Müller, and N. Livesey (2010), Annual cycle of ozone at and above the tropical tropopause: Observations versus simulations with the chemical model of the stratosphere (CLaMS), *Atmos. Chem. Phys.*, *10*, 121–132.

Lacis, A. A., D. J. Wuebbles, and J. A. Logan (1990), Radiative forcing of climate by changes in the vertical distribution of ozone, *J. Geophys. Res.*, *95*(D7), 9971–9981.

Lorenz, E. N. (1963), Deterministic non-periodic flow, *J. Atmos. Sci.*, *20*, 130–141.

Mahowald, N. M., R. A. Plumb, P. J. Rasch, J. del Corral, and F. Sassi (2002), Stratospheric transport in a three-dimensional isentropic coordinate model, *J. Geophys. Res.*, *107*(D15), 4254, doi:10.1029/2001JD001313.

McKenna, D. S., P. Konopka, J.-U. Grooß, G. Günther, R. Müller, R. Spang, D. Offermann, and Y. Orsolini (2002a), A new Chemical Lagrangian Model of the Stratosphere (CLaMS): 1. Formulation of advection and mixing, *J. Geophys. Res.*, *107*(D16), 4309, doi:10.1029/2000JD000114.

McKenna, D. S., J.-U. Grooß, G. Günther, P. Konopka, R. Müller, G. Carver, and Y. Sasano (2002b), A new Chemical Lagrangian Model of the Stratosphere (CLaMS): 2. Formulation of chemistry scheme and initialization, *J. Geophys. Res.*, *107*(D15), 4256, doi:10.1029/2000JD000113.

Offermann, D., K.-U. Grossmann, P. Barthol, P. Knieling, M. Riese, and R. Trant (1999), Cryogenic Infrared Spectrometers and Telescopes for the Atmosphere (CRISTA) experiment and middle atmosphere variability, *J. Geophys. Res.*, *104*(D13), 16,311–16,325, doi:10.1029/1998JD100047.

Pan, L. L., P. Konopka, and E. V. Browell (2006), Observations and model simulations of mixing near the extratropical tropopause, *J. Geophys. Res.*, *111*, D05106, doi:10.1029/2005JD006480.

Ploeger, F., P. Konopka, G. Günther, J.-U. Grooß, and R. Müller (2010), Impact of the vertical velocity scheme on modeling transport in the tropical tropopause layer, *J. Geophys. Res.*, *115*, D03301, doi:10.1029/2009JD012023.

Ploeger, F., et al. (2011), Insight from ozone and water vapor on transport in the tropical tropopause layer (TTL), *Atmos. Chem. Phys.*, *11*, 401–419, doi:10.5194/acp-11-407-2011.

Randel, W. J., M. Park, L. Emmons, D. Kinnison, P. Bernath, K. Walker, C. Boone, and H. Pumphrey (2010), Asian monsoon transport of pollution to the stratosphere, *Science*, *328*, 611–613.

Rap, A., P. M. Forster, A. Jones, O. Boucher, J. M. Haywood, N. Bellouin, and R. R. De Leon (2010), Parameterization of contrails in the UK Met Office Climate Model, *J. Geophys. Res.*, *115*, D10205, doi:10.1029/2009JD012443.

Riese, M., X. Tie, G. Brasseur, and D. Offermann (1999), Three-dimensional simulation of stratospheric trace gas distributions measured by CRISTA, *J. Geophys. Res.*, *104*(D13), 16,419–16,435, doi:10.1029/1999JD900178.

Riese, M., G. L. Manney, J. Oberheide, X. Tie, R. Spang, and V. Kuell (2002), Stratospheric transport by planetary wave mixing as observed during CRISTA-2, *J. Geophys. Res.*, *107*(D23), 8179, doi:10.1029/2001JD000629.

Riese, M., F. Friedl-Vallon, R. Spang, P. Preusse, C. Schiller, L. Hoffmann, H. Oelhaf, T. von Clarmann, and M. Höpfner (2005), Global Limb Radiance Imager for the Atmosphere (GLORIA): Scientific objectives, *Adv. Space Res.*, *36*(5), 989–995.

Rossow, W. B., and R. A. Schiffer (1999), Advances in understanding clouds from ISCCP, *Bull. Am. Meteorol. Soc.*, *80*, 2261–2288.

Simmons, A., S. Uppala, D. Dee, and D. Kobayashi (2006), ERA-Interim: New ECMWF reanalysis products from 1989 onwards, *ECMWF Newsl.*, *110*, 25–35.

Solomon, S., K. H. Rosenlof, R. W. Portman, J. S. Daniel, S. M. Davis, T. J. Sanford, and G.-K. Plattner (2010), Contributions of stratospheric water vapor to decadal changes in the rate of global warming, *Science*, *327*, 1219–1223, doi:10.1126/science.1182488.

SPARC CCMVal (2010), SPARC report on the evaluation of chemistry-climate models, edited by V. Eyring, T. G. Shepherd, and D. W. Waugh, *WMO/TD-No. 1526*, WMO, Geneva, Switzerland.

Sparling, L. C. (2000), Statistical perspectives on stratospheric transport, *Rev. Geophys.*, *38*, 417–436, doi:10.1029/1999RG000070.

Stenke, A., V. Grewe, and M. Ponater (2008), Lagrangian transport of water vapor and cloud water in the ECHAM4 GCM and its impact on the cold bias, *Clim. Dyn.*, *31*(5), 491–506, doi:10.1007/s00382-007-0347-5.

Stevenson, D. S., et al. (2006), Multimodel ensemble simulations of present-day and near-future tropospheric ozone, *J. Geophys. Res.*, *111*, D08301, doi:10.1029/2005JD006338.

Vogel, B., et al. (2011), Transport pathways and signatures of mixing in the extratropical tropopause region derived from Lagrangian model simulations, *J. Geophys. Res.*, *116*, D05306, doi:10.1029/2010JD014876.

von Hobe, M., et al. (2011), Evidence for heterogeneous chlorine activation in the tropical UTLS, *Atmos. Chem. Phys.*, *11*, 241–256.

Zhang, Y., W. B. Rossow, A. A. Lacis, V. Oinas, and M. L. Mishchenko (2004), Calculation of radiative fluxes from the surface to top of atmosphere based on ISCCP and other global data sets: refinement of the radiative transfer model and the input data, *J. Geophys. Res.*, *109*, D19105, doi:10.1029/2003JD004457.